Effective electron displacements: A tool for time-dependent density functional theory computational spectroscopy

C.A. Guido, P. Cortona, C. Adamo

Effective electron displacements: A tool for time-dependent density functional theory computational spectroscopy

Ciro A. Guido,[1,a)] Pietro Cortona,[1] and Carlo Adamo[2,3]
[1]*Laboratoire Structures, Propriétés et Modélisation des Solides (SPMS), CNRS UMR 8580, École Centrale Paris, Grande Voie des Vignes, F-92295 Châtenay-Malabry, France*
[2]*Laboratoire d'Électrochimie, Chimie des Interfaces et Modélisation pour l'Energie, CNRS UMR-7575, Chimie ParisTech, 11 rue P. et M. Curie, F-75231 Paris Cedex 05, France*
[3]*Institut Universitaire de France, 103 Bd Saint-Michel, F-75005 Paris, France*

(Received 27 November 2013; accepted 14 February 2014; published online 10 March 2014)

We extend our previous definition of the metric Δr for electronic excitations in the framework of the time-dependent density functional theory [C. A. Guido, P. Cortona, B. Mennucci, and C. Adamo, J. Chem. Theory Comput. **9**, 3118 (2013)], by including a measure of the difference of electronic position variances in passing from occupied to virtual orbitals. This new definition, called Γ, permits applications in those situations where the Δr-index is not helpful: transitions in centrosymmetric systems and Rydberg excitations. The Γ-metric is then extended by using the Natural Transition Orbitals, thus providing an intuitive picture of how locally the electron density changes during the electronic transitions. Furthermore, the Γ values give insight about the functional performances in reproducing different type of transitions, and allow one to define a "confidence radius" for GGA and hybrid functionals. © *2014 AIP Publishing LLC*. [http://dx.doi.org/10.1063/1.4867007]

I. INTRODUCTION

The modeling of excited electronic states is the first step in order to study many complex problems in physics, chemistry, biology, and material science, such as solar energy devices,[1] photochemistry,[2] laser control,[3] vision,[4] photosynthesis,[5] and many others. Accurate post-Hartree-Fock (post-HF) methods, such as Coupled Cluster (CC), Multi Reference Configuration Interaction (MRCI), or Complete Active Space second-order Perturbation Theory (CASPT2), just to cite a few, are powerful tools for interpreting and even predicting electronic spectra, but increasing the size of the systems they become computationally too expensive for medium and large systems. On the other hand, approximate, yet more flexible approaches, such as Time Dependent Density Functional Theory[6,7] (TD-DFT), are characterized by an optimal ratio between accuracy and computational cost for transition involving valence electrons. However, the TD-DFT approach sums up the typical problems of ground state DFT with those originating in the Linear Response (LR) approximation and the adiabatic assumption, in particular in describing charge transfer (CT) excitations, multielectron excitations, and absorption spectra of systems with delocalized or not-paired electrons, as extensively shown in literature for vertical excitation energies[8–12] and optimized geometries.[13–15] In order to analyze the performances of TD-DFT simulations, some numerical tools were developed and applied.[16–21] They include geometrical descriptors as well as indexes based on the analysis of the molecular orbitals or the electron densities. All these descriptors have pros and cons, and some of them have been used as diagnostic tools in order to monitor the accuracy of TD-DFT results.[16–18,21] Very recently, we introduced a new metric[21] (Δr) based on a simple quantity, the charge centroid,[22] in order to define a trust, or convergence, radius for molecular excitation calculations performed in the framework of TD-DFT. The interest of the Δr-index resides in its chemically simple pictorial meaning (hole-particle separation) and in the straightforward evaluation (at negligible computational cost). In this contribution, we extend our previous definition of the metric in order to take in account those situations where the Δr-index has showed an unsatisfactory discrimination power, such as centrosymmetric molecules and Rydberg excitations. The final definition of the new index is based on the Natural Transition Orbitals (NTO),[23] in order to further simplify its chemical interpretation in difficult cases. Furthermore, the effect of the basis set as well as that of the selected exchange-correlation functionals on the new descriptor has been investigated, thus providing evidence of the high discrimination power between short- and long-range excitations of the proposed index. The paper is organized as follows: in Sec. II after a brief recall of the definition of Δr, we introduce the variance of the orbital centroids to define Γ and the corresponding Γ_{NTO} index based on NTOs; in Sec. III the computational details are reported; in Sec. IV results over the training sets of CT and Rydberg excitations are discussed. Concluding remarks are reported in Sec. V.

II. THEORY

The Δr index has been defined as[21]

$$\Delta r = \frac{\sum_{ia} K_{ia}^2 |\langle \varphi_a | \mathbf{r} | \varphi_a \rangle - \langle \varphi_i | \mathbf{r} | \varphi_i \rangle|}{\sum_{ia} K_{ia}^2}, \quad (1)$$

a)Electronic mail: ciro.guido@ecp.fr

where $\varphi_p|\mathbf{r}|\varphi_p$ is an orbital centroid,[22] and

$$K_{ia} = X_{ia} + Y_{ia} \tag{2}$$

includes both excitation (X_{ia}) and de-excitation (Y_{ia}) coefficients and refers to the Random Phase Approximation (RPA) formulation of TD-DFT,[6]

$$\begin{bmatrix} \mathbf{A} & \mathbf{B} \\ \mathbf{B} & \mathbf{A} \end{bmatrix} \begin{bmatrix} \mathbf{X} \\ \mathbf{Y} \end{bmatrix} = \omega \begin{bmatrix} 1 & 0 \\ 0 & -1 \end{bmatrix} \begin{bmatrix} \mathbf{X} \\ \mathbf{Y} \end{bmatrix}. \tag{3}$$

The molecular orbital indexes follow the usual convention: i, j, k, l… for occupied states; a, b, c, d… for virtual; p, q, r, s… for generic orbitals. This index represents the average hole-particle distance covered during the excitation, weighted in function of the excitation coefficients. This metric allows one to discriminate between valence and charge transfer states, and to define threshold values in order to individuate short- and long-ranged excitations.[21] However, according to the definition of Eq. (1), the index value is zero in centrosymmetric systems. Moreover, transitions to Rydberg states could not be characterized by large distances between centroids of the involved orbitals. Strictly speaking, an electron is not localized on the orbital centroid, but is smeared out in the region of space of the associated orbital. A rough measure of this delocalization around the centroid can be defined as the root mean square deviation of the position operator

$$\sigma_p = \sqrt{\langle\varphi_p|\mathbf{r}^2|\varphi_p\rangle - \langle\varphi_p|\mathbf{r}|\varphi_p\rangle^2}. \tag{4}$$

This suggests the definition the new index as

$$\Gamma = \Delta r + \Delta\sigma = \frac{\sum_{ia} K_{ia}^2 |\langle\varphi_a|\mathbf{r}|\varphi_a\rangle - \langle\varphi_i|\mathbf{r}|\varphi_i\rangle|}{\sum_{ia} K_{ia}^2} + \frac{\sum_{ia} K_{ia}^2 |\sigma_a - \sigma_i|}{\sum_{ia} K_{ia}^2}, \tag{5}$$

where

$$\Delta\sigma = \frac{\sum_{ia} K_{ia}^2 |\sigma_a - \sigma_i|}{\sum_{ia} K_{ia}^2}. \tag{6}$$

The definition in Eq. (5) reduces to $\Delta\sigma$ in Eq. (6) for excitations in centrosymmetric systems. Moreover, $\Delta\sigma$ is expected to be more sensitive than Δr in describing excitations that involve transitions to more diffuse orbitals, such as the Rydberg excitations.

In many cases, there are no dominant configurations in the list of excitation and de-excitation amplitudes (X_{ia} and Y_{ia}), thus the identification of the excited state nature is difficult, and a simple orbital interpretation of "what got excited to where" is not straightforward. The analysis in term of NTOs provides an approach to this problem that relies on finding a compact orbital representation for the electronic transition density matrix.[23] By applying separate unitary transformations to the occupied and the virtual orbitals (the corresponding orbital transformation of Amos and Hall[24]) a maximal correspondence between the excited "particle" and the empty "hole" can be obtained, without changing the transition density. Once the NTOs are calculated, the corresponding Γ metric reduces to

$$\Gamma_{NTO} = \Delta r_{NTO} + \Delta\sigma_{NTO} = \frac{\sum_{ia}^{Nocc} \lambda_{ia} |\langle\phi_a|\mathbf{r}|\phi_a\rangle - \langle\phi_i|\mathbf{r}|\phi_i\rangle|}{\sum_{ia}^{Nocc} \lambda_{ia}} + \frac{\sum_{ia}^{Nocc} \lambda_{ia} |\sigma_a^{NTO} - \sigma_i^{NTO}|}{\sum_{ia}^{Nocc} \lambda_{ia}}. \tag{7}$$

In Eq. (7), ϕ represents a NTO and λ_{ia} is the corresponding eigenvalue associated with the hole-particle ($i \rightarrow a$) amplitude. Each eigenvalue reflects the importance of a particular particle-hole excitation. The eigenvalue sum is identically equal to one in the Tamm-Dancoff approximation[25] (TDA), but in RPA will deviate from that to the extent that the de-excitations are significant. However, these last terms are usually small (and this explains the success of TDA in reproducing TDDFT). Usually, only one or two eigenvalues are very large, accounting for more of the 90% of the nature of the excitation.[23]

III. BENCHMARK SETS AND COMPUTATIONAL DETAILS

All DFT and TD-DFT calculations have been carried out with a locally modified version of the GAUSSIAN development program,[26] where Γ and Γ_{NTO} were implemented.

The implementation is really simple: given the first and second moments of the atomic orbitals, usually calculated and stored at the end of the self-consistent field (SCF) calculation, the routines combine these integrals using coefficients coming from SCF, TD-DFT, and NTO calculations.

Two test sets (reported in Figure 1), including molecules having different type of excitations, have been chosen. The first set, already used to calibrate Δr,[21] includes systems presenting challenging CT excitations,[16] namely: a model dipeptide, longer chains β-dipeptide and tripeptide, and N-phenylpyrrole (PP), for a total of 12 CT and 9 valence excitations. The second set contains systems presenting Rydberg excited states: N_2, CO, H_2CO, acetone, benzene, and pyridine, for a total of 28 Rydberg and 15 valence excitations. Finally, some large chromophores such as Triazene II (7 excitations), 11-cis-retinal (2 excitations), and 11-cis-dihydroretinal (3 excitations) have been considered as applications of the new indexes.

The structures reported in the benchmark repository[27] were used for the first training set and N_2, CO, H_2CO molecules, whereas for pyridine and acetone the structures were optimized at the MP2/6-311+G** level, as done in Ref. 9. The D_{6h} structure with $r_{CC} = 1.392$ Å and $r_{CH} = 1.086$ Å, as reported in Refs. 28 and 29, was used to compute excitation energies of benzene.

In the case of Triazene II,[30] the geometry was optimized using the same functional (and basis set) as in the calculation of the electronic transitions. The B3LYP/6-31+G(d) structures were used for both 11-cis-retinal and 11-cis-dihydroretinal.[31]

In the present work, we limit our analysis to one Generalized Gradient Approximation (GGA) and two Global Hybrid (GH) functionals: PBE,[32] PBE0,[33,34] and PBE0-1/3.[35,36] Our

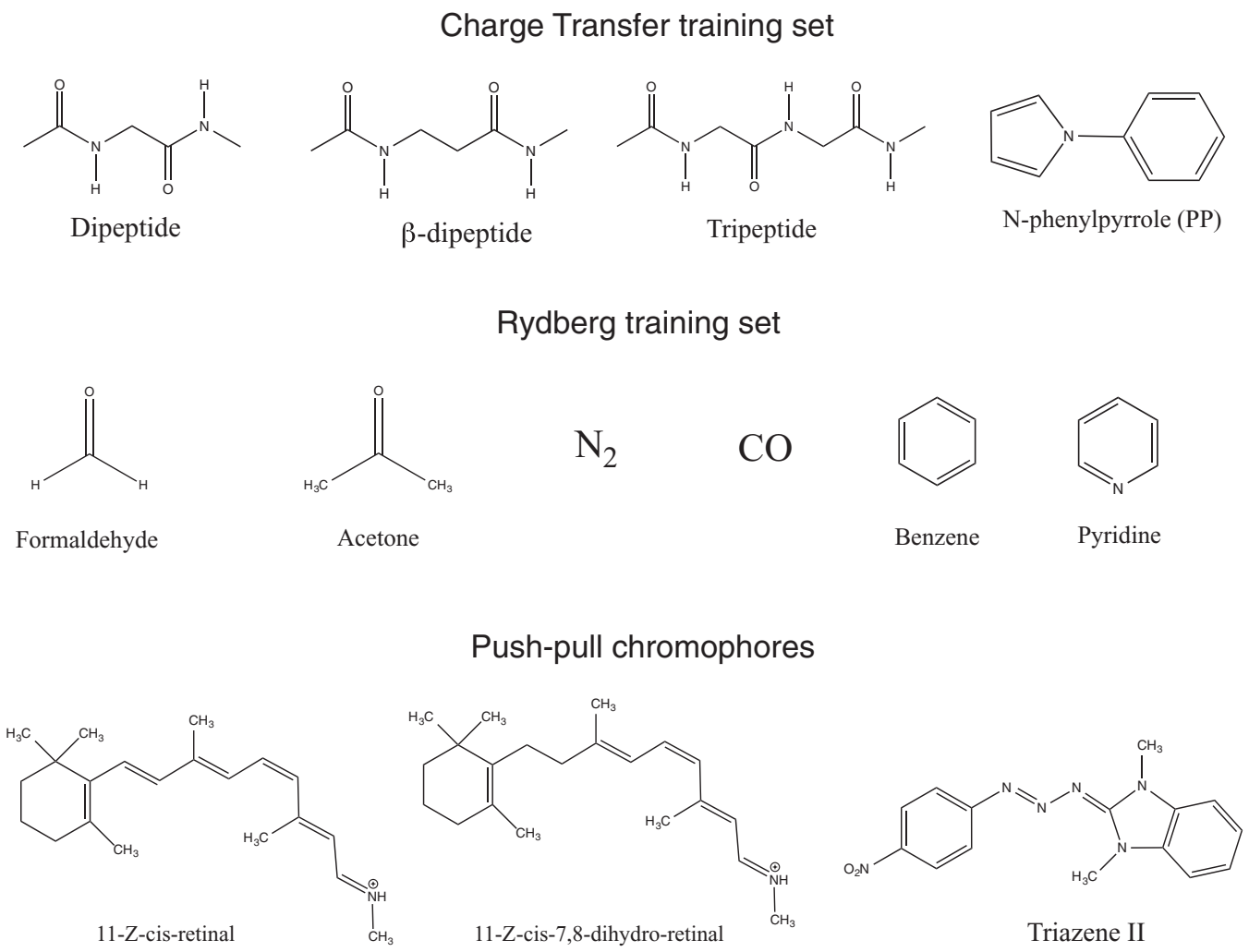

FIG. 1. The sets of molecular systems considered in the present study.

choice is motivated by the fact that we have already shown[21] that the performances of hybrid functionals with a HF exchange (HF-X) percentage greater than or equal to 50% are almost uncorrelated to the index values, as for range separated hybrid (RSH) functionals. Moreover, from our precedent work[21] we can also expect that functionals belonging to the same family (i.e., GGAs, meta-GGAs, or GHs with close values of HF-X percentage) give similar results.

Basis set effects have been studied using three different basis sets in simulating excitations of the first two sets of molecules. In particular, cc-pVTZ, 6-311++G(2d,2p), and aug-cc-pVTZ were selected for the CT test set; while 6-311++G(2d,2p), aug-cc-pVTZ, and d-aug-cc-PVTZ were used for the Rydberg test set. The total number of functions, together with the number of diffuse functions for each system and for each basis set is reported in Table I. Calculations for Triazene II and both 11-cis-retinal and 11-cis-dihydroretinal were performed by PBE0/6-311+G(2d,p) and PBE0/6-31++G(d,p), respectively.

The excitation reference values were taken from the literature. In particular, results of CASPT2 were considered for model peptides, while, in the PP case, the results come from CC2/cc-pVTZ calculations. In both cases, the reference values are issued from Ref. 16. Experimental gas-phase results were used for the systems of the Rydberg training set: for N_2 and CO, the results are issued from Ref. 16; for H_2CO and acetone we refer to the experimental results used in both benchmarks of Caricato *et al.*[9] and Isegawa *et al.*[37] Finally, for benzene and pyridine, we use the reference values reported by Adamo *et al.*[29] The assignment of the valence and CT states was checked by looking at the orbitals mainly involved in the transition. The Rydberg states are more difficult to assign. As suggested in Ref. 9 and applied in Ref. 37, for each molecule we sorted both experimental and calculated states in energy order within each irreducible representation to compare them. RI-CC2/def-QZVPP results were considered for Triazene II[30] and RI-CC2/def-SV(P) for both 11-cis-retinal and 11-cis-dihydroretinal.[31]

IV. RESULTS AND DISCUSSION

A. Basis set effects on the Δr-index

Let us start by considering the effect of the basis set on the original descriptor, Δr. In our previous paper,[21] we used the cc-pVTZ basis set and we argued that, since TD-DFT calculations of CT excitations are sensible to basis set effects,[38] a slight extension of the upper bound of Δr upon inclusion of

TABLE I. Total number of functions and number of diffuse functions included in each basis set, for both training sets of molecules we have considered.

CT test set		cc-pVTZ		6-311++G(2d,2p)		aug-cc-pVTZ	
System	No. of e^-	Total	No. of diffuse	Total	No. of diffuse	Total	No. of diffuse
Dipeptide	70	410	0	343	46	644	234
β-Dipeptide	78	468	0	390	52	736	268
Tripeptide	100	572	0	481	65	897	325
PP	76	456	0	387	53	713	257
Rydberg test set		6-311++G(2d,2p)		aug-cc-pVTZ		d-aug-cc-pVTZ	
System	No. of e^-	Total	No. of diffuse	Total	No. of diffuse	Total	No. of diffuse
N_2	14	54	8	92	32	124	64
CO	14	54	8	92	32	124	64
H_2CO	16	74	10	138	50	188	100
Acetone	32	168	22	322	118	440	236
Benzene	42	222	30	414	132	546	264
Pyridine	42	212	29	391	141	532	282

diffuse functions could be expected and therefore we retained the interval 1.5–2.0 Å as threshold for short/long range interactions. Here, we numerically show that our precedent conclusion was correct by comparing results for different basis sets.

In Figure 2, the absolute deviations (|ΔE|, in eV) of TD-DFT calculations as a function of Δr are reported, with different basis sets including diffuse functions. As shown in the figure, the inclusion of diffuse functions causes a shift toward larger Δr values. This is particularly true when the HF-X percentage in the functional increases. Indeed, GGA values of Δr (and the corresponding |ΔE| values) are quite insensitive to the inclusion of diffuse functions: the average variation (for both 6-311++G(2d,2p) and aug-cc-pVTZ with respect to

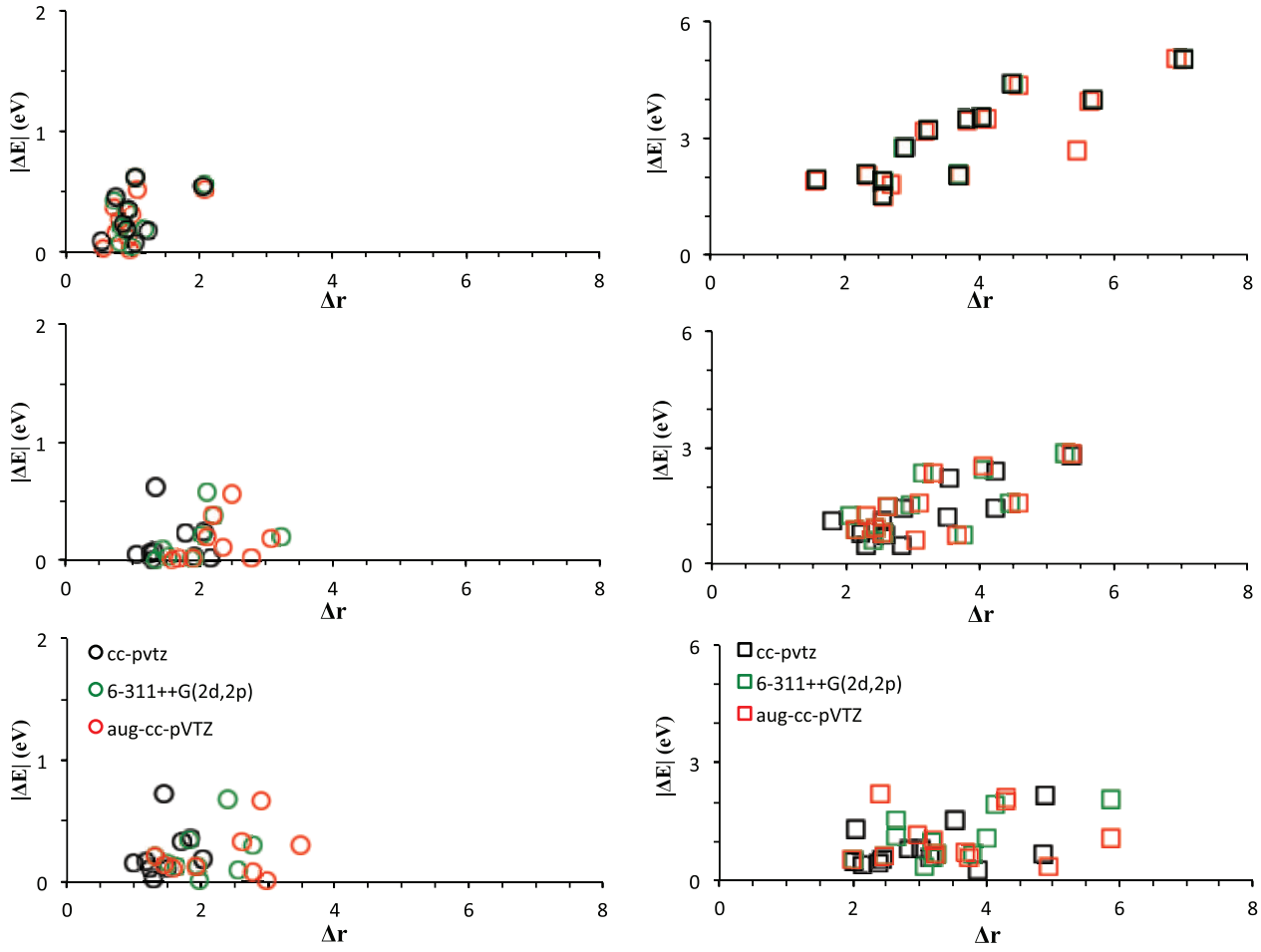

FIG. 2. Unsigned excitation energy deviations (|ΔE|, eV) plotted against the Δr index (Å) for the CT training set (see Figure 1). Calculations have been made with different basis set: cc-pVTZ (in black), 6-311++G(2d,2p) (in green), and aug-cc-pVTZ (in red). Left side: valence excitations; right side: charge transfer excitations. Top: PBE functional; middle: PBE0 hybrid functional; bottom: PBE0-1/3 hybrid functional.

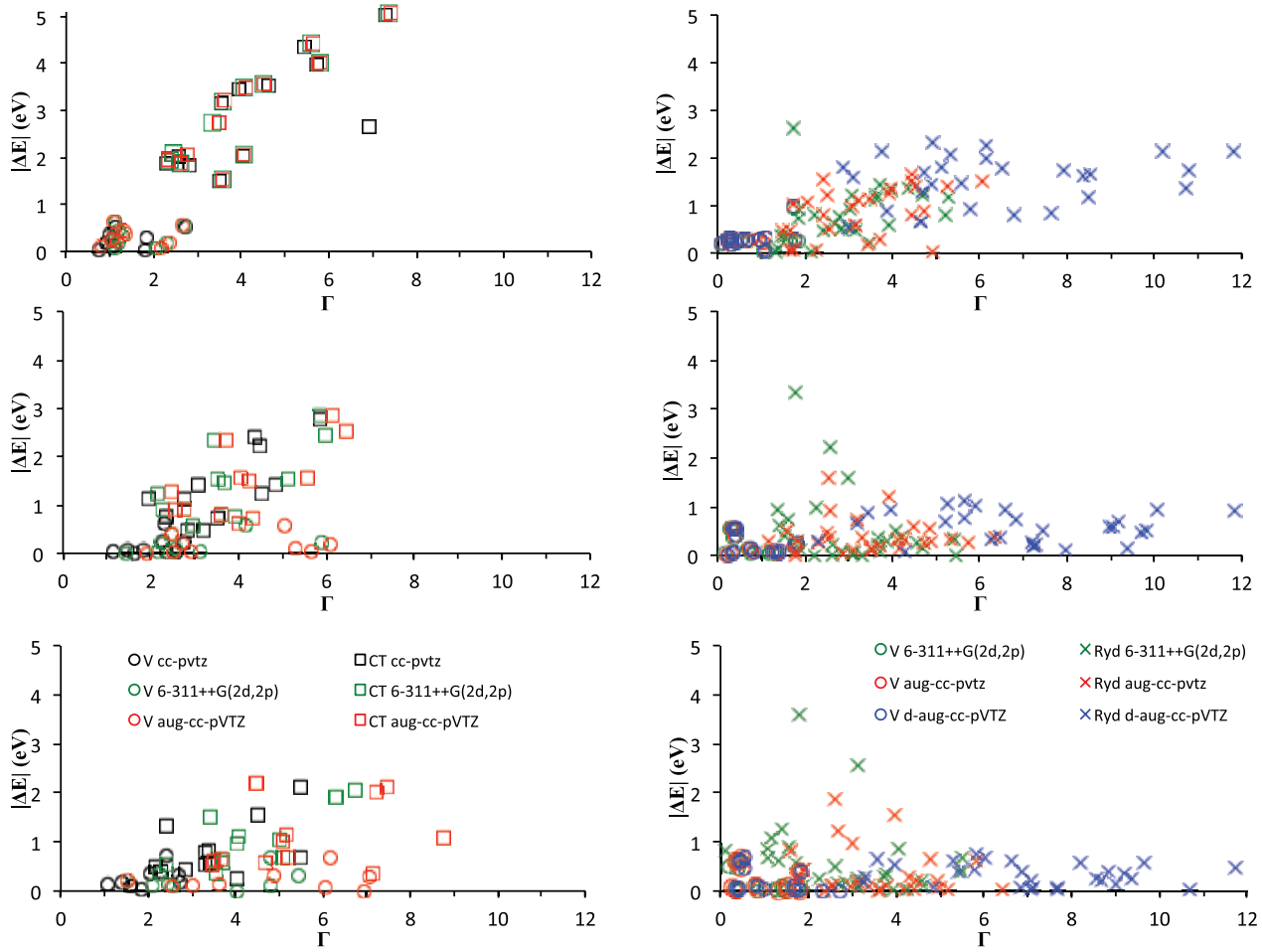

FIG. 3. Unsigned excitation energy deviations (|ΔEl, eV) plotted against the Γ-index (Å) for the CT and Rydberg training sets (see Figure 1). Left side: valence and charge transfer excitations with the cc-pVTZ (in black), 6-311++G(2d,2p) (in green), and aug-cc-pVTZ (in red) basis sets; right side: valence and Rydberg excitations with the 6-311++G(2d,2p) (in green), aug-cc-pVTZ (in red), and d-aug-cc-pVTZ (in blue) basis sets. Top: PBE functional; middle: PBE0 hybrid functional; bottom: PBE0-1/3 hybrid functional.

cc-pVTZ) of Δr is less than 0.1 Å for valence excitations and less than 0.3 Å for the CT ones. Coherently, the mean absolute deviations of excitation energy change less than 0.1 eV for both CT and valence transitions.

For PBE0, the values are larger: in going from cc-pVTZ to 6-311++G(2d,2p) and from cc-pVTZ to aug-cc-pVTZ, the mean variations of the metric for valence states are 0.39 Å and 0.66 Å, respectively, and they are 0.37 Å and 0.44 Å in the case of CT excitations. In this case, the mean absolute deviation (MAD) of excitation energy changes of about 0.1 eV for valence and 0.16 eV for CT states. Finally, the shift toward larger values of Δr increasing the number of diffuse functions is accentuated in PBE0-1/3: in going from cc-pVTZ to 6-311++G(2d,2p) and from cc-pVTZ to aug-cc-pVTZ, the mean variations of the metric are, respectively, 0.59 Å and 0.93 Å for valence states and 0.59 Å and 0.62 Å for the CT ones. Mean absolute deviations of excitation energy change around 0.1 eV for valence and 0.25 eV for CT states.

It should be noted that also with the larger 6-311++G(2d,2p) and aug-cc-pVTZ basis sets all the CT excitations show values greater than 1.5 Å for PBE, and 2.0 Å for PBE0, and PBE0-1/3. Absolute deviations lower than (or close to) 0.5 eV are found for values of Δr shorten than these thresholds. The interval 1.5–2.0 Å as Δr threshold for short/long range interactions can be then retained, thus confirming our precedent conclusions. However, the large dependence of Δr upon diffuse functions for some valence excitations can be reduced introducing NTOs as we show in Secs. IV B–IV D.

B. Γ-index behavior

The new metric Γ, as defined by Eq. (5), has been validated for valence, CT, and Rydberg states, considering different basis sets, and the results are shown in Figure 3. At first glance, we note that the new index, Γ, shows some discrimination abilities also for the description of the Rydberg excited states, by the inclusion of $\Delta\sigma$ in its definition. This is particularly true for those systems with a center of inversion such as nitrogen and benzene molecules, which cannot be discriminated with the original descriptor, since $\Delta r = 0$ by definition. Indeed a threshold appears around 2 Å: Γ below this value indicates valence excitations, whereas larger values can be attributed to Rydberg excitations. A clear differentiation cannot be done, instead, between valence and CT transitions, even if the same onset value (2 Å) appears. As

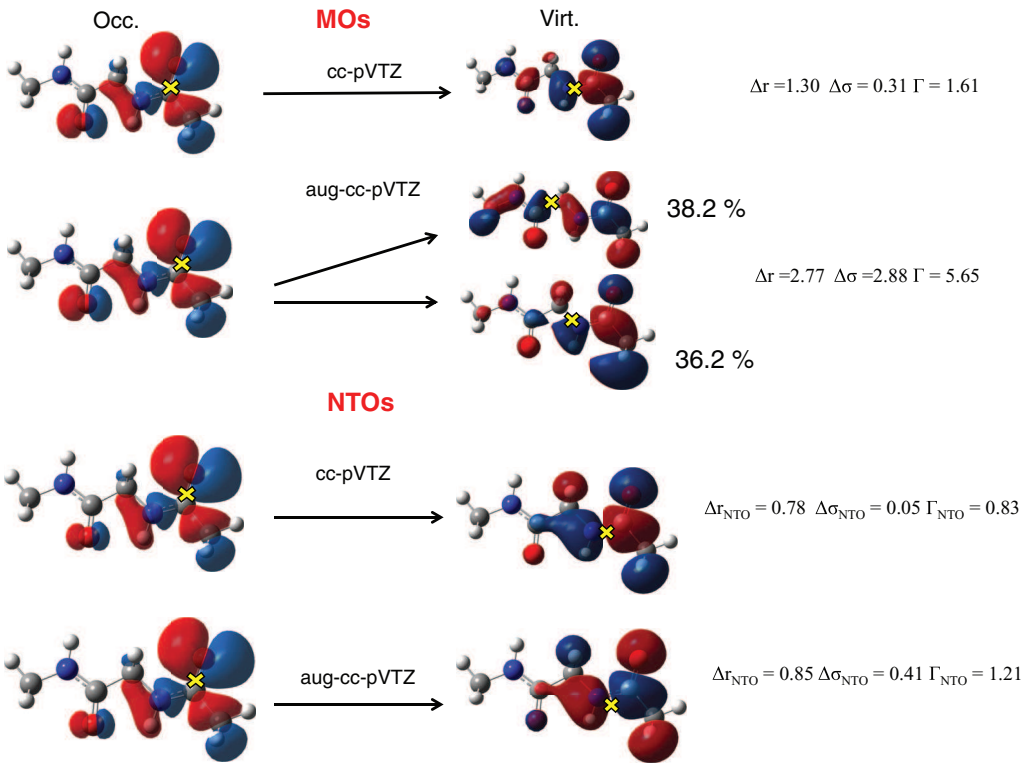

FIG. 4. Effect of adding diffusion functions over the PBE0 isosurfaces (isovalue of 0.02 a.u.) of the molecular orbitals involved in the description of the first (valence) excited state of model dipeptide. The corresponding NTO isosurfaces (isovalue of 0.02 a.u.) are reported in the bottom part of the figure. The yellow "x" indicates the orbital centroid. The Γ and Γ_{NTO} values are in Å.

already stated before, the effect of adding diffuse functions in the basis set used for CT excitations is greater in the case of hybrids functionals: PBE excitations energies are practically already converged using cc-pVTZ (including diffuse functions change the MAD of 0.05 eV), whereas for the PBE0 and PBE0-1/3 CT excitations we found a change of MAD of 0.15 eV and 0.25 eV, respectively. As expected, the role of diffuse function becomes dramatically larger in the case of Rydberg excitations: in passing from 6-311++G(2d,2p) to d-aug-cc-pVTZ, MAD change of 0.77, 0.53, and 0.45 eV for PBE, PBE0, and PBE0-1/3, respectively. Moreover, in passing from aug-cc-pVTZ to d-aug-cc-pVTZ, MAD change of 0.66, 0.33, and 0.35 eV for PBE, PBE0, and PBE0-1/3, respectively. As for Δr, we observe very large Γ-values for valence excited states of the molecules in the CT test set using hybrid functionals, which could make difficult its use for verifying functional performances. We first note that this really large sensitivity to the diffuse functions in the basis set used is manly found for systems that present π-chains in their structure.

The reasons of this behavior of the Γ–metric can be illustrated considering the case of the model dipeptide. In the upper part of Figure 4, the PBE0 molecular orbitals involved in the description of the first (valence) excited state of the model dipeptide are reported, for both cc-pVTZ and aug-cc-pVTZ bases. These plots clearly show that the addition of diffuse functions produces more delocalized virtual molecular orbitals. Coherently, the values of both Δr and Δσ indexes (and therefore Γ) obtained with the aug-cc-pVTZ are greater than those found with the smaller basis set (cc-pVTZ) even if the two bases give similar excitation energies (5.59 eV and 5.62 eV, respectively).

C. Index on the basis of NTO's: Γ_{NTO}

The precedent results point out the difficulties in assignment of TD-DFT, sometimes related to the orbital description. In this context, NTOs appear not only as a useful interpretative tool but also as a natural basis for the expression of our indexes. This can be pictorially showed by the analysis of the mentioned transition in the model dipeptide (Figure 4, lower part). Indeed, the analysis in terms of NTOs clearly shows a maximal correspondence between the excited "particle" and the empty "hole," showing that actually the involved NTOs are not really different between the simulations with cc-pVTZ and the larger aug-cc-pVTZ. The absolute TD-DFT deviations (|ΔE|) as a function of Γ_{NTO} are reported in Figure 5. We no longer include the 6-311++G(2d,2p) results in our analysis, as we have already noted that for CT systems they are very similar to the aug-cc-pVTZ ones and that for Rydberg calculations they are very far from the convergence. We consider the behavior of the various functionals for the valence excitations subsets. PBE gives 0.5 Å $\leq \Gamma_{NTO} \leq$ 3.0 Å, but most of the values are smaller than 2 Å, i.e., the range of values found for the GHs PBE0 and PBE0-1/3: 0.5 Å $\leq \Gamma_{NTO} \leq$ 2.0 Å. Valence excitations do not really need diffuse functions: coherently we found converged results for both excitation energies and Γ_{NTO} values adding these functions to the basis set. On the contrary, CT and, even more, Rydberg excitations are really sensitive to the inclusion of diffuse functions. The

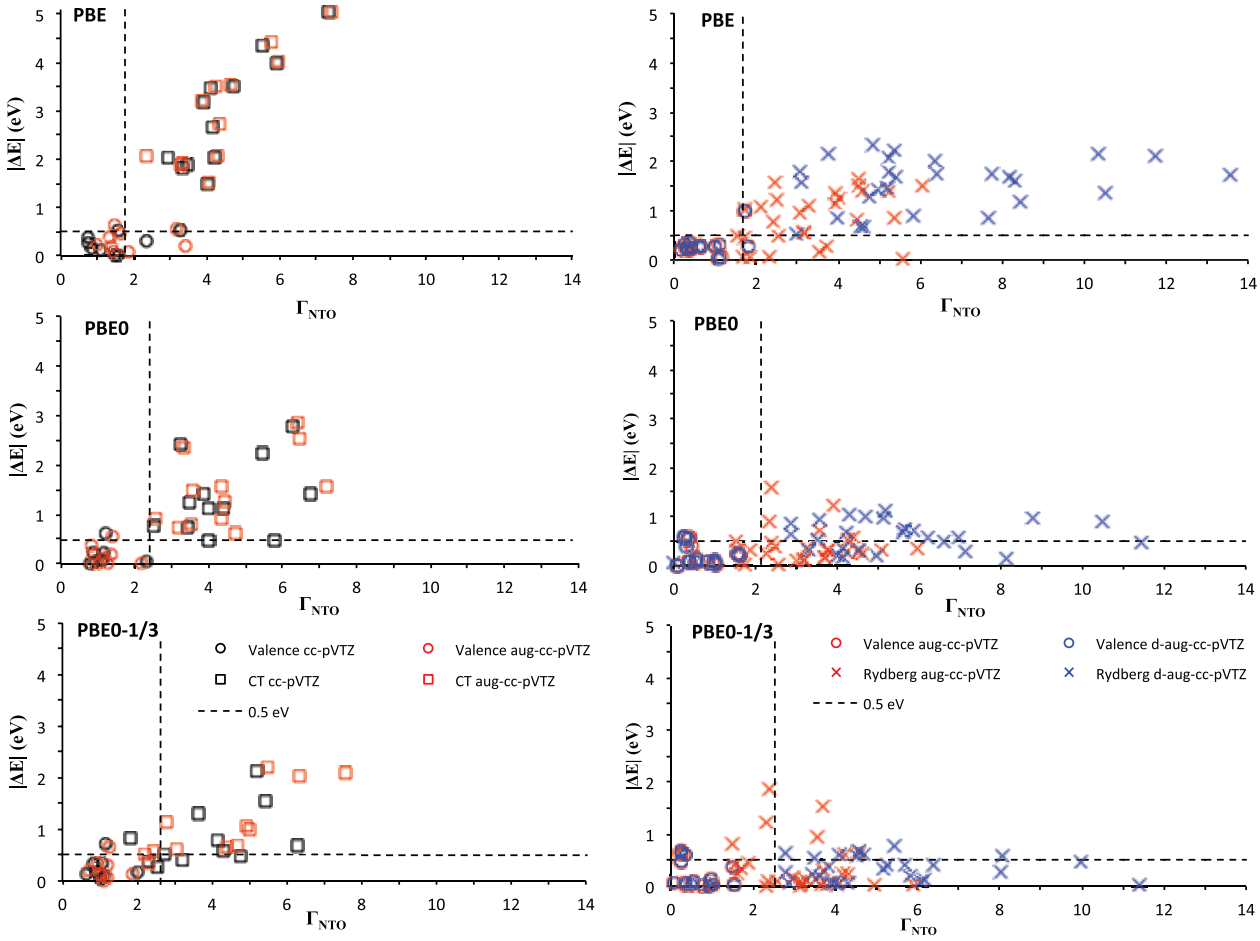

FIG. 5. Unsigned excitation energy deviations (|ΔEl, eV) plotted against the Γ_{NTO}-index (Å) for the CT and Rydberg training sets (see Figure 1). Left side: valence and charge transfer excitations with the cc-pVTZ (in black), 6-311++G(2d,2p) (in green), and aug-cc-pVTZ (in red) basis sets; right side: valence and Rydberg excitations with the 6-311++G(2d,2p) (in green), aug-cc-pVTZ (in red), and d-aug-cc-pVTZ (in blue) basis sets. Top: PBE functional; middle: PBE0 hybrid functional; bottom: PBE0-1/3 hybrid functional. Dashed lines: horizontal lines are placed at 0.5 eV; vertical lines represent the threshold values of Γ_{NTO}.

choice of the threshold values monitoring the functional performances is therefore done using the larger basis sets, i.e., aug-cc-pVTZ for CT (red squares) and d-aug-cc-pVTZ for Rydberg (blue "x"s).

Analyzing the excitations it appears that, for GGA and GHs with HFX percentage lower or equal to 33%, errors increase with the increasing of the effective distance covered during the excitation: $|\Delta E| > 0.5$ eV if $\Gamma_{NTO} > 1.8$ Å for PBE, or if $\Gamma_{NTO} > 2.40$ Å for PBE0. This threshold value increases for larger HF contributions, and it becomes 2.55 Å in the case of PBE0-1/3. Interestingly, the reciprocal of these distances are 0.29, 0.22, and 0.21 Bohr^{-1} for PBE, PBE0, and PBE0-1/3, respectively. These values are really close to those determined by Rohrdanz *et al.*[39] for the parameter ω of long range corrected PBE-based functionals in varying the fixed percentage of HF-X included from 0 to 0.3. This parameter represents the inverse of the cutoff radius of the short/long range part of the Coulomb interaction and therefore should not be unexpected that the Γ_{NTO} thresholds are close to the empirically fitted values of ω. Moreover, in the same line, we observe that increasing the HF-X percentage, the short-range threshold increases (or, alternatively, the ω-parameter decreases).

As a final comment, let us illustrate in Figure 6 the contributions of Δr_{NTO} and $\Delta\sigma_{NTO}$ to Γ_{NTO} in the case of PBE0 (but the results are obviously similar for PBE and PBE0-1/3). As already stated, Δr_{NTO} for systems with an inversion center (such as N_2 and benzene) is zero and, more important, values for Rydberg states are in the same range as the valence ones. The effect of $\Delta\sigma_{NTO}$ is the clear introduction of a distinction between CT and Rydberg excitations that, as expected, present very large values of the variance of the centroids. We finally note that the performances of PBE0-1/3 clearly show that a percentage around 30% of HF-X should be enough in order to properly describe Rydberg excitations without deteriorating the valence ones: mean absolute deviations for the Rydberg training set of systems are 0.22 eV and 0.33 eV, respectively, for valence and Rydberg excitations using PBE0-1/3; 0.21 eV and 0.58 eV, respectively, for valence and Rydberg excitations using PBE0; 0.28 eV and 1.51 eV, respectively, for valence and Rydberg excitations using PBE. Therefore, for Rydberg excitations we cannot expect a strong relation between the functional performances and the metric values in the case of global hybrids functionals, but only for GGA.

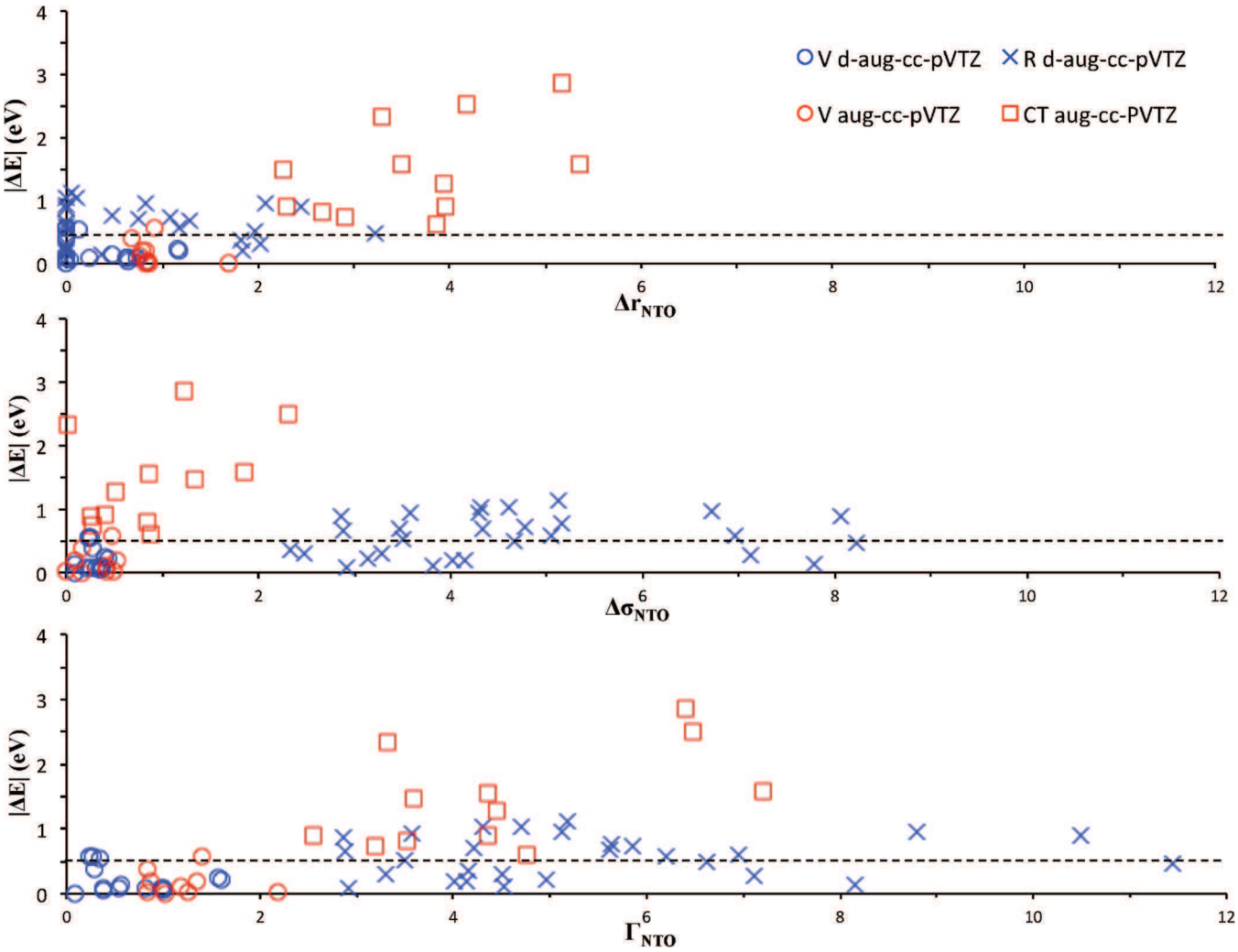

FIG. 6. PBE0 unsigned excitation energy deviations (|ΔE| in eV) as a function of the Δr_{NTO} (top), $\Delta\sigma_{NTO}$ (middle), and Γ_{NTO} (bottom) indices (Å) for the CT and Rydberg training sets (see Figure 1). Horizontal dashed lines are placed at 0.5 eV.

In general, Γ_{NTO} can differentiate valence excitations, while Δr_{NTO} and $\Delta\sigma_{NTO}$ provide a detailed analysis between the CT and the Rydberg nature of states.

D. Large chromophores

Once calibrated, we can now check the performances of the Γ_{NTO} metric in the case of some large push pull chromophores. In Figure 7, PBE0 results are reported for Triazene II, 11-cis-retinal, and 11-cis-dihydro-retinal. These extended systems present charge delocalization and are particularly difficult cases for TD-DFT. Triazene II was studied by Preat *et al.*[40] and its excitation energies were analyzed in terms of absolute overlap (Λ) by Peach *et al.*:[30] they showed that, in this case, Λ does not provide a clear indication of the functional performances. In our precedent work,[21] we applied the Δr metric showing that all these excitations involve a hole-electron distance greater than 2.0 Å thus large errors can be expected for non-range-separated functionals. Here, we confirm these results, showing that the introduction of Γ_{NTO} permits also to recover a more linear behavior between the increase of the error and the increase of the metric index. The two retinal chromophores are prototypal examples of how a simple chemical change can lead to a significant reduction in TD-DFT accuracy: Zaari and Wong[31] observed that B3LYP low-lying excitation energies and oscillator strengths were in reasonable agreement with the RI-CC2 reference values for

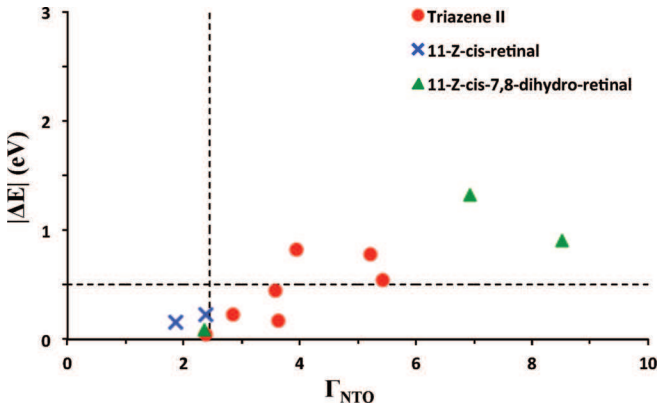

FIG. 7. PBE0 unsigned excitation energy deviations (|ΔE| in eV) of Triazene II, 11-cis-retinal, and 11-cis-dihydro-retinal excitation energies as a function of the Γ_{NTO}-index (Å).

the 11-cis-retinal, but large discrepancies were found after hydrogenation. Later, Dwyer and Tozer[41] showed that the excitation energy errors are readily understood by considering how the orbitals and their overlap are affected by hydrogenation. Figure 7 shows that PBE0 has a behavior similar to the B3LYP one and that this behavior can be analyzed in terms of the effective displacements by Γ_{NTO}: the first two excited states of 11-cis-retinal and the second excitation of the hydrogenate analogue are short ranged in nature ($\Gamma_{NTO} < 2.4$ Å) and deviations with respect to the RI-CC2 values are small (less than 0.3 eV). On the contrary, the first and third excited states of 11-cis-dihydro-retinal are long ranged and large deviations with respect to RI-CC2 are found.

V. FINAL COMMENTS AND CONCLUSIONS

We have extended our previous definition of a metric index for molecular excitations in order to define an effective hole-particle distance covered during the excitations. The new index is the sum of two contributions: the orbital centroid distance and the variation of the electron delocalization around each centroid of the involved orbitals. Coupling this definition with a NTO description, we are able to extract a maximal correspondence between the excited "particle" and the empty "hole" and to quantify it with a negligible computational cost. In other words this procedure permits to identify the "principal components" of the transition electron density (by using NTO) and provide a measure of the interaction distance of the hole-particle pairs. We have related the new metric to the functional performances and tested the new index with different basis sets, kind of excitations (valence, Rydberg, and CT), and functionals, thus providing evidence of the high discrimination power between short- and long-range excitations of the proposed index. The interest of this Γ_{NTO}–index resides in its ability to provide a reliable diagnostic of performances on one hand and to describe of the nature of excitations provided by TD-DFT calculations on the other.

We suggest using Γ_{NTO} to individuate excitations that are likely to be prone to large errors (i.e., $\Gamma_{NTO} > 1.8$ Å for GGAs and $\Gamma_{NTO} > 2.4$ Å for Global Hybrids with 20%–30% of HF-X percentage), and Δr_{NTO} and $\Delta\sigma_{NTO}$ to provide a detailed analysis between the CT and the Rydberg nature of states.

The analysis presented here can also be used in order to quantify solvent effects and/or geometry relaxations following excitations, and these ones will be the subjects of our future work.

ACKNOWLEDGMENTS

This work has been supported by the ANR agency under the project Dinf DFT (Project No. ANR 2010 BLANC n. 0425).

[1] B. O'Regan and M. Grätzel, Nature (London) **353**, 737 (1991).
[2] M. J. Molina and F. S. Rowland, Nature (London) **249**, 810 (1974).
[3] K. Moore and H. Rabitz, Nat. Chem. **4**, 72 (2012).
[4] G. Wald, Nature (London) **219**, 800 (1968).
[5] G. R. Fleming and G. D. Scholes, Nature (London) **431**, 256 (2004).
[6] M. E. Casida, in *Recent Advances in Density Functional Methods. Part I*, edited by D. P. Chong (World Scientific, Singapore, 1995), pp. 155–193.
[7] E. Runge and E. K. U. Gross, Phys. Rev. Lett. **52**, 997 (1984).
[8] D. Jacquemin, V. Wathelet, E. A. Perpète, and C. Adamo, J. Chem. Theory Comput. **5**, 2420 (2009).
[9] M. Caricato, G. W. Trucks, M. J. Frisch, and K. B. Wiberg, J. Chem. Theory Comput. **6**, 370 (2010).
[10] M. A. Rohrdanz and J. M. Herbert, J. Chem. Phys. **129**, 034107 (2008).
[11] L. Goerigk, J. Moellmann, and S. Grimme, Phys. Chem. Chem. Phys. **11**, 4611 (2009).
[12] L. Goerigk and S. Grimme, J. Chem. Phys. **132**, 184103 (2010).
[13] C. A. Guido, D. Jacquemin, C. Adamo, and B. Mennucci, J. Phys. Chem. A **114**, 13402 (2010).
[14] C. A. Guido, S. Knecht, J. Kongsted, and B. Mennucci, J. Chem. Theory Comput. **9**, 2209 (2013).
[15] D. Bousquet, R. Fukuda, P. Maitarad, D. Jacquemin, I. Ciofini, C. Adamo, and M. Ehara, J. Chem. Theory Comput. **9**, 2368 (2013).
[16] M. J. G. Peach, P. Benfield, T. Helgaker, and D. J. Tozer, J. Chem. Phys. **128**, 044118 (2008).
[17] T. Le Bahers, C. Adamo, and I. Ciofini, J. Chem. Theory Comput. **7**, 2498 (2011).
[18] H. Nitta and I. Kawata, Chem. Phys. **405**, 93 (2012).
[19] M. J. Bedard-Hearn, F. Sterpone, and P. J. Rossky, J. Phys. Chem. A **114**, 7661 (2010).
[20] F. Plasser and H. Lischka, J. Chem. Theory Comput. **8**, 2777 (2012).
[21] C. A. Guido, P. Cortona, B. Mennucci, and C. Adamo, J. Chem. Theory Comput. **9**, 3118 (2013).
[22] J. M. Foster and S. F. Boys, Rev. Mod. Phys. **32**, 300 (1960).
[23] R. L. Martin, J. Chem. Phys. **118**, 4775 (2003).
[24] A. T. Amos and G. G. Hall, Proc. Roy. Soc. **A263**, 483 (1961).
[25] A. L. Fetter and J. D. Walecka, *Quantum Theory of Many-Particle Systems* (McGraw-Hill, New York, 1971).
[26] M. J. Frisch, G. W. Trucks, H. B. Schlegel *et al.*, Gaussian 09, Revision H11, Gaussian, Inc., Wallingford, CT, 2009.
[27] See http://www.dur.ac.uk/d.j.tozer/excite3.html for more information.
[28] N. C. Handy and D. J. Tozer, J. Comput. Chem. **20**, 106 (1999).
[29] C. Adamo, G. E. Scuseria, and V. Barone, J. Chem. Phys. **111**, 2889 (1999).
[30] M. J. G. Peach, C. R. Le Sueur, K. Ruud, M. Guillaume, and D. J. Tozer, Phys. Chem. Chem. Phys. **11**, 4465 (2009).
[31] R. R. Zaari and S. Y. Y. Wong, Chem. Phys. Lett. **469**, 224 (2009).
[32] J. P. Perdew, K. Burke, and M. Ernzerhof, Phys. Rev. Lett. **77**, 3865 (1996).
[33] C. Adamo and V. Barone, J. Chem. Phys. **110**, 6158 (1999).
[34] M. Ernzerhof and G. E. Scuseria, J. Chem. Phys. **110**, 5029 (1999).
[35] P. Cortona, J. Chem. Phys. **136**, 086101 (2012).
[36] C. A. Guido, E. Brémond, C. Adamo, and P. Cortona, J. Chem. Phys. **138**, 021104 (2013).
[37] M. Isegawa, R. Peverati, and D. G. Truhlar, J. Chem. Phys. **137**, 244104 (2012).
[38] I. Ciofini and C. Adamo, J. Phys. Chem. A **111**, 5549 (2007).
[39] M. A. Rohrdanz, K. M. Martins, and J. M. Herbert, J. Chem. Phys. **130**, 054112 (2009).
[40] J. Preat, C. Michaux, A. Lewalle, E. A. Perpète, and D. Jacquemin, Chem. Phys. Lett. **451**, 37 (2008).
[41] A. D. Dwyer and D. J. Tozer, Phys. Chem. Chem. Phys. **12**, 2816 (2010).